

SUPERSONIC DIFFUSION USING
HYDRAULIC ANALOGY

by
C. L. Murphy

Thesis submitted in partial fulfillment
of the requirements for the degree of
Master of Engineering

Department of Mechanical Engineering
McGill University
Montreal
April 1960

LIST OF FIGURES

	Figure
1. Location of Measuring Positions	43
2. Diagram of Supersonic Wedge and Perforated Diffuser .	44
3. Side view of Hydraulic Analogue	45
4. End view of Hydraulic Analogue	46
5. Model in Test Section of Hydraulic Analogue	47
6. Two Methods of Photographing Surface Waves	48
7. Flow Pattern with and without Perforation Spillage ..	49
8. Illustration of Bow Wave	50
9. Comparison of Contraction Ratios required to swallow an Hydraulic jump with and without Perforation Spillage	51
10. Swallowing Hydraulic Jump by increasing the Inlet Mach number	52
11. Froude Number vs. Height Ratio across Sluice Nozzle .	53
12. Froude Number vs. Height Ratio for Supersonic Water Pitot	54
13. Froude Number vs. Mass Flow Ratio	55
14. Froude Number and Mach Number vs. Oblique Shock Angle for Water and a Gas	56
15. Froude Number and Mach Number vs. Area Contraction Ratio for Water and a Gas	57
16. Experimental and theoretical results of a Perforated Diffuser	58
17. Carpet Plot comparison of the Theoretical and Experimental Perforated Diffuser Results	59

NOMENCLATURE

A	Area
c	Wave propagation velocity
f	Function of
F	Froude number
g	Acceleration of gravity
h	Water depth
m	Mass flow
M	Mach number
p	Static pressure
R	Gas constant
T	Absolute gas temperature
V	Local fluid velocity
W	Width of water diffuser
γ	Ratio of specific heats
β	Oblique shock angle
α	Wedge angle
λ	Wave length
ρ	Density
σ	Surface tension
Subscripts	
c	Refers to open channel
g	Refers to a gas
w	Refers to water
o	Refers to isentropic stagnation conditions or upstream nozzle conditions.
x	Refers to conditions before shock or hydraulic jump
y	Refers to conditions after shock or hydraulic jump

ACKNOWLEDGEMENTS

The author would like to express his thanks to Professor J.H.T. Wu and Dr. B.G. Newman for their guidance and advice.

Thanks are also due to; Mr. F. Corrick for his advice in the construction of the apparatus, and Miss Janine Lacroix for typing this thesis.

The financial assistance given by the Department of Mechanical Engineering is gratefully acknowledged.

SUMMARY

A water channel was constructed and calibrated in order to carry out tests on a supersonic perforated diffuser using the hydraulic analogy.

It was found that the boundary layer effects and height ratios of water flows could not be simulated accurately to the theoretical boundary layer effects and pressure ratios for two-dimensional gas flows. However a good comparison of contraction ratios could be obtained.

The contraction ratio necessary to swallow the hydraulic jump in a perforated diffuser was determined at seven inlet Froude numbers and various mass flow recovery factors. The Froude number was varied between 1.6 and 2.5 with a mass flow recovery factor ranging from 100 to 75 percent.

A theoretical relation between the inlet Mach number, the mass flow recovery factor and the area contraction ratio to swallow a shock was developed for an ideal gas flow. It was assumed in the derivation that the ratio of specific heats was equal to 1.4 and that the Mach number at the throat was equal to 1 with the shock at the inlet of the diffuser.

Photographs of the two-dimensional flow patterns in the diffuser were obtained at various positions of the hydraulic jump.

1 INTRODUCTION AND REVIEW

The testing of a supersonic perforated diffuser model in a water channel has not been done before to the author's knowledge. The main advantage of using the hydraulic analogue, besides its economic one, is the ease by which the flow conditions and diffuser geometry can be altered. Mass flows can also be obtained by direct measurement with relative ease.

Models of supersonic perforated diffusers have been tested in wind tunnels (refs. 1, 2 and 3). However these tests have been limited on each model to one contraction ratio and the corresponding isentropic inlet Mach number. Mass flow spillage through the perforations was calculated from theoretical consideration of the pressure ratio, position of the shock in the diffuser and the area and location of the perforations. The controlled variables, for a given Mach number and contraction ratio, were the number and placement of the perforations and the back pressure. Variations of the inlet Mach number, the contraction ratio, and the spillage mass flow would be very costly and difficult to obtain from wind tunnel tests. However the interdependence of such parameters could easily be obtained by testing a diffuser in a water channel.

The results obtained from tests on a diffuser model using an hydraulic analogue are limited in their application to an ideal two-dimensional gas flow diffuser. The limitations are implied by assumptions inherent in the analogy. It was therefore

necessary to make a thorough study of the hydraulic analogy before the test results could be applied intelligently to a gas flow.

Models of machines that operate in air have been tested in water channels for many years. G. A. Crocco carried out tests with models of trains and airships in water as long ago as 1906. The works of D. Riabouchinsky in 1932 and the more detailed studies of E. Preiswerk in 1944 (Ref. 4) laid down the fundamental relationships for the air-water analogy. These relationships have not changed to the present time. However refinements and additional theory have been developed more recently. The advent of high speed flight has created more interest in the hydraulic analogy as a means of testing supersonic models.

A. H. Shapiro (Ref. 5) found that, with reference to supersonic flow, the hydraulic analogy was limited to qualitative studies, and quantitative studies of a comparative nature.

A study of the relationships between Mach interactions in a gas and hydraulic jumps was carried out by H. E. Crossley Jr. using a water table (Ref. 6). He found a definite disagreement between experimental results and the theory of H. A. Einstein and E. G. Baird for the interaction of hydraulic jumps of the Mach reflection type.

The hydraulic analogue has also been studied for various flow conditions other than supersonic. Dynamical similarities of models in water and in air were investigated

by Giulio Supino (Ref. 7). The analogy was studied for subsonic flow extending into the critical region by W. Orlin, N. Gindner and J. Bitterly (Ref. 8). They found close agreement of pressure distributions and flow fields for the analogy but were not able to obtain quantitative accuracy. Unsteady flow relations of the analogy have also been investigated (Ref. 16). It was found that the ratio of specific heats could be varied, for the analogy, by varying the shape of the channel cross-section from the standard rectangular shape.

A study of a supersonic converging-diverging wedge diffuser in an hydraulic analogue was carried out at the Massachusetts Institute of Technology under A. H. Shapiro (Ref. 9). The limiting contraction ratio for starting and choking the diffuser at various diffuser angles was determined. Close agreement with one dimensional analysis was found for starting the diffuser. The contraction ratio necessary for choking or expelling the hydraulic jump did not agree as closely with the one-dimensional analysis. A description of the hydraulic analogue used for these tests on the supersonic diffuser has been given by K. Goldman and S. Meerbaum (Ref. 10).

2. THEORETICAL ANALYSIS

The hydraulic analogy is theoretically determined from similarities of the basic flow equations for a compressible gas and for a free surface water flow. The basis of the supersonic flow analogy is the comparison between the speed of sound in a gas and the speed of a gravity wave in shallow water.

The relationships obtained for the analogy from the perfect gas, energy, continuity and momentum equations have been derived (Refs. 4, 11 and 12). The basic assumptions used in the analogy are:

1. An isentropic gas with a specific heat ratio of 2.
2. The gas flow is steady two-dimensional and irrotational.
3. The water flow is steady, two-dimensional and frictionless.

2.1 Fundamental Relationships

For certain conditions of water flow (section 2.2) the velocity of a gravity wave is

$$c_w = \sqrt{g h} \quad (1)$$

The corresponding speed of a pressure wave in a gas is

$$c_g = \sqrt{g \gamma R T} \quad (2)$$

The Froude number in hydraulics is

$$F = \frac{V}{c_w} \quad (3)$$

and the corresponding Mach number in gas dynamics is

$$M = \frac{V}{c_g} \quad (4)$$

The Froude number is analogous to the Mach number. Therefore from equations (1) to (4) it can be seen that $h \propto T$ if g , γ , and R are constant and,

$$\frac{T}{T_0} = \frac{h}{h_0} \quad (5)$$

The continuity equation for the two-dimensional steady water flow is

$$\frac{\partial (h v_x)}{\partial x} + \frac{\partial (h v_y)}{\partial y} = 0 \quad (6)$$

and the corresponding equation for gas flow is

$$\frac{\partial (\rho v_x)}{\partial x} + \frac{\partial (\rho v_y)}{\partial y} = 0 \quad (7)$$

From (6) and (7) it can be seen that

$$\frac{\rho}{\rho_0} = \frac{h}{h_0} \quad (8)$$

For a perfect gas

$$\frac{\rho}{\rho_0} = \left(\frac{T}{T_0}\right)^{\frac{1}{\gamma-1}} \quad (9)$$

From equations (5) and (8)

$$\frac{\rho}{\rho_0} = \frac{T}{T_0} \quad (10)$$

Equations (9) and (10) are both satisfied when $\gamma = 2$.

For a perfect gas

$$\frac{p}{p_0} = \left(\frac{T}{T_0}\right)^{\frac{\gamma}{\gamma-1}} \quad (11)$$

Equations (5) and (11) with $\gamma = 2$ give

$$\frac{p}{p_0} = \left(\frac{h}{h_0}\right)^2 \quad (12)$$

Equations (1) and (2), (3) and (4), (5), (8) and (12) are the fundamental relations for the hydraulic analogy.

A general examination of the assumptions made in the analogy are given by A. H. Shapiro (Ref. 5). The deviations of the analogy will be discussed with particular reference to the test results obtained on the supersonic perforated diffuser.

2.2 Determination of the Froude Number

The Froude number is equal to the simulated Mach number for the hydraulic analogy. In order to avoid confusing the simulated Mach number for water with the Mach number for a gas the Froude number will be used when referring to water flows.

The velocity of a gravity wave is equal to $\sqrt{g h}$ only under certain conditions. The general equation for the velocity of a surface wave is

$$c_w^2 = \left(\frac{g \lambda}{2 \pi} + \frac{2 \pi \sigma}{\lambda} \right) \tanh \frac{2 \pi h}{\lambda} \quad (13)$$

If the wave length (λ) is large compared to the water depth (h), as in gravity waves, then the surface tension (σ) is negligible compared to the gravity force (g). Therefore from equation (13)

$$\frac{c_w^2}{g h} = \frac{\lambda}{2 \pi h} \tanh \frac{2 \pi h}{\lambda} \quad (13a)$$

In the limit as $\frac{\lambda}{h} \rightarrow \infty$, $\frac{c_w^2}{g h} \rightarrow 1$ and $c_w \rightarrow \sqrt{g h}$

If the wave length is small compared to the water depth, as in capillary waves, then the gravity force is negligible compared to the capillary force and from equation (13)

$$h c_w^2 = \frac{2 \pi \sigma h}{\lambda} \tanh \frac{2 \pi h}{\lambda} \quad (13b)$$

In the limit as $\frac{\lambda}{h} \rightarrow 0$, $h c_w^2 \rightarrow \infty$ and $c_w \rightarrow \infty$

At water depths of approximately 0.25 inches the variation of the wave velocities was found to be negligible (Ref. 5). At this water depth $\frac{\lambda}{h}$ is such that the velocity of gravity waves, and capillary waves with wave lengths greater than .05 inches, are equal to $\sqrt{g h}$. Water depths of 0.25 inches were used in the hydraulic analogue therefore $c_w = \sqrt{g h}$ and from equation (3)

$$F = \frac{V}{g h} \quad (14)$$

The Froude number can now be obtained by five different methods.

(a) The Froude number can be obtained as a function of the stagnation water depth and the exit water depth across a water nozzle.

Referring to figure 1b and applying the energy equation.

$$h_0 + \frac{V_0^2}{2g} = h + \frac{V^2}{2g} \quad (15)$$

Combining equations (14) and (15) and neglecting V_0

$$\frac{h}{h_0} = \frac{2}{F^2 + 2} \quad (16)$$

This relation was plotted in figure 11.

Two assumptions were made in the derivation.

First that $V_0 = 0$, and secondly that there was no loss of energy through the nozzle due to friction. The value of V_0 can be calculated by a trial and error process. Knowing the Mach number from the first approximation, V_0 can be obtained. The value of $V_0^2/2g$ can then be added to h_0 and a second approximation obtained for h/h_0 and hence M .

The loss of energy, due to friction through the nozzle, can be compensated for to a certain extent by sloping the channel.

(b) The Froude number can be obtained as a function of the water depths using a supersonic water pitot as shown in figure 1b.

Applying the continuity and energy equations across the hydraulic jump

$$\text{Continuity } h_x V_x = h_y V_y \quad (17)$$

$$\text{Momentum } V_x h_x (V_x - V_y) + g h_x \left(\frac{h_x - h_y}{2} \right) = V_y h_y (V_y - V_x) + g h_y \left(\frac{h_x - h_y}{2} \right) \quad (18)$$

$$\text{and } V_x^2 h_x - V_y^2 h_y = \frac{g}{2} (h_y^2 - h_x^2) \quad (18a)$$

Re-arranging and combining (17) and (18a)

$$V_x^2 = \frac{g h_x}{2} \frac{h_y}{h_x} \left(\frac{h_y}{h_x} + 1 \right) \quad (19)$$

From equations (14) and (19)

$$F_x^2 = \frac{1}{2} \frac{h_y}{h_x} \left(\frac{h_y}{h_x} + 1 \right) \quad (20)$$

$$\text{or } F_y^2 = \frac{1}{2} \frac{h_x}{h_y} \left(\frac{h_x}{h_y} + 1 \right) \quad (20a)$$

The energy equation from position y to o (figure 1b) is

$$\frac{h_o^1}{h_y} = 1 + \frac{F_y^2}{2} \quad (21)$$

Combining equations (20a) and (21)

$$\frac{h_o^1}{h_x} = \frac{h_y}{h_x} + \frac{1}{4} + \frac{h_x}{4 h_y} \quad (22)$$

Then from equations (20) and (22)

$$F_x = f\left(\frac{h_y}{h_x}\right) = f\left(\frac{h_x}{h_o'}\right) \quad (23)$$

and F_x can be plotted as a function of h_x/h_o' figure 12.

It was assumed in this derivation that there was no loss of energy between the positions of h_y and h_o' . This loss, as in the previous relation, can be compensated for by sloping the channel.

(c) The Froude number can be obtained as a function of the mass flow of water, the depth of the water in the channel test section and the cross-sectional area of the water in the channel test section. From the continuity equation

$$m = \rho A V \quad (24)$$

Rearranging equation (24) and combining with equation (14)

$$F = \frac{m}{\rho A \sqrt{g h}} \quad (25)$$

and assuming ρ and g are constant

$$F = f\left(\frac{m}{A \sqrt{h}}\right) \quad (25a)$$

This relationship is plotted in figure 13.

(d) The Froude number can be obtained as a function of the oblique shock angle from a supersonic wedge.

Referring to figure 2a and applying the continuity equation across the oblique shock

$$h_x V_{x_n} = h_y V_{y_n} \quad (26)$$

from figure 2a

$$\tan \beta = \frac{V_{x_n}}{V_{x_t}} \text{ and } \tan (\beta - \Delta) = \frac{V_{y_n}}{V_{y_t}}$$

$$\frac{h_y}{h_x} = \frac{V_{x_t} \tan \beta}{V_{y_t} \tan (\beta - \Delta)} \quad (27)$$

but the velocity along the oblique shock is constant

$$\frac{h_y}{h_x} = \frac{\tan \beta}{\tan (\beta - \Delta)} \quad (28)$$

from the momentum equation (19)

$$V_{x_n}^2 = \frac{g h_x}{2} \frac{h_y}{h_x} \left(\frac{h_y}{h_x} + 1 \right) \quad (29)$$

from figure 2a $V_{x_n} = \sin \beta V_x$ (30)

$$V_x^2 = \frac{1}{\sin^2 \beta} \left(\frac{g h_x}{2} \right) \frac{h_y}{h_x} \left(\frac{h_y}{h_x} + 1 \right) \quad (31)$$

and $F_x^2 = \frac{1}{2 \sin^2 \beta} \frac{h_y}{h_x} \left(\frac{h_y}{h_x} + 1 \right)$ (32)

from equations (28) and (32) and taking Δ as a constant

$$F_x = f\left(\frac{h_y}{h_x}\right) = f(\beta)$$

F_x is plotted as a function of β for a 10° wedge angle (Δ) in figure 14.

(e) The Froude number can be obtained as a function of the width ratio necessary to swallow an hydraulic jump from its position at the inlet. Referring to figure 2b and applying the continuity equation

$$W_1 h_x V_x = W_1 h_y V_y = W_2 h_2 V_2 \quad (33)$$

$$\text{and} \quad \frac{W_1}{W_2} = \frac{h_2 V_2}{h_x V_x} \quad (33a)$$

from equation (14) and taking $V_2 = \sqrt{g h}$, with the hydraulic jump at the inlet of the diffuser.

$$\frac{W_1}{W_2} = \frac{h_2}{h_x} \frac{1}{F_x} \frac{\sqrt{g h_2}}{\sqrt{g h_x}} = \left(\frac{h_2}{h_y}\right)^{3/2} \left(\frac{h_y}{h_x}\right)^{3/2} \frac{1}{F_x} \quad (34)$$

From the energy equation

$$\frac{h_{0y}}{h_y} = 1 + \frac{F_y^2}{2} \quad \text{and} \quad \frac{h_{02}}{h_2} = 1 + \frac{1}{2} \quad (35)$$

$$\text{and} \quad \frac{h_2}{h_y} = \left(\frac{h_{02}}{h_{0y}}\right) \left(\frac{1 + \frac{F_y^2}{2}}{1 + \frac{1}{2}}\right) \quad (36)$$

If the energy is assumed constant from y to 2

$$\text{then } \frac{h_2}{h_y} = \frac{2 + F_y^2}{3} \quad (37)$$

substituting equation (37) in (34) and

$$\frac{W_1}{W_2} = \left(\frac{h_y}{h_x}\right)^{3/2} \left(\frac{2 + F_y^2}{3}\right)^{3/2} \left(\frac{1}{F_x}\right) \quad (38)$$

and from the equations (20) and (20a) for an hydraulic jump

$$\frac{W_1}{W_2} = f\left(\frac{h_y}{h_x}\right) = f(F_x) \quad (39)$$

This relation was plotted in figure 15.

2.3 Determination of the Mach Number Relations

The Mach number was determined, as a function of the oblique shock angle and the area contraction ratio necessary for swallowing a shock from its position at the inlet. The relations were determined for an ideal two-dimensional gas with specific heat ratios of 1.4 and 2.

For the oblique shock relations the following equations may be derived from the standard gas equations (Ref. 12). Referring to figure 2a

$$\frac{\rho_y}{\rho_x} = \frac{\tan \beta}{\tan (\beta - \delta)} \quad (40)$$

$$\frac{p_y}{p_x} = \frac{\frac{\gamma+1}{\gamma-1} \left(\frac{\rho_y}{\rho_x}\right) - 1}{\frac{\gamma+1}{\gamma-1} - \frac{\rho_y}{\rho_x}} \quad (41)$$

$$M_x = \frac{\frac{p_y}{p_x} - 1}{\gamma \sin^2 \beta \left(1 - \frac{\rho_x}{\rho_y}\right)} \quad (42)$$

From the above three relations M_x was plotted as a function of β for $\delta = 10^\circ$ with $\gamma = 2$ (Figure 14).

The area contraction ratio necessary for swallowing the shock from its position at the inlet was obtained from the standard gas equations. (Ref. 12). Referring to figure 2a

$$\left(\frac{A_1}{A_2}\right)_y = \left(\frac{A_1}{A_2}\right)_x \left(\frac{p_{0y}}{p_{0x}}\right) \quad (43)$$

where
$$\frac{A_1}{A_2} = \frac{1}{M_x} \left[\left(\frac{2}{\gamma+1}\right) \left(1 + \frac{\gamma-1}{2} M_x^2\right) \right]^{\frac{\gamma+1}{2(\gamma-1)}} \quad (44)$$

and
$$\frac{p_{0y}}{p_{0x}} = \left[\frac{\frac{\gamma+1}{2} M_x^2}{1 + \frac{\gamma-1}{2} M_x^2} \right]^{\frac{\gamma}{\gamma-1}} \left[\frac{2\gamma}{\gamma+1} M_x^2 - \frac{\gamma-1}{\gamma+1} \right]^{\frac{1}{1-\gamma}} \quad (45)$$

From the above three relations the contraction ratio $\left(\frac{A_1}{A_2}\right)$ required to swallow a shock for an ideal isentropic gas with $\gamma = 1.4$ and $\gamma = 2$ was plotted in figure 15.

2.4 Deviations of the Analogy

Quantitative water flow results cannot be directly applied to gas flows using the hydraulic analogy because of assumptions that were used in the analogy. However, quantitative water flow results of a comparative nature can be applied to gas flows with a greater degree of accuracy (Ref. 5).

The effect of assuming an inviscid fluid and gas in the analogy is undetermined. The characteristics of the boundary layer in the fluid are difficult to determine experimentally because of the low water velocities, which are about one foot per second. Theoretical comparisons between the boundary layers of a gas and a liquid are too complex to use in the analogy.

The frictional effect on the channel floor can be compensated for by sloping the channel, as mentioned previously (section 2.2). The amount of slope can be determined by allowing the hydraulic jump to pass down the channel until the water depth becomes constant. However this will compensate for the frictional effects for only one given water depth. If there is a variation in the water depth, as there is when a model is placed in the channel, then the frictional effect on the channel bottom will vary with the water depth. This variation of the frictional effects is undetermined.

The deviations between flow parameters for a gas with $\gamma = 1.4$ and an analogous gas with $\gamma = 2$ can be seen in figures 14 and 15.

The analogy for hydraulic jumps in water and shocks in a gas with $\gamma = 2$ does not hold true (Ref. 5). Across a shock the stagnation temperature is constant, however across an hydraulic jump the total head suffers a decrease. The decrease in the total head is due to eddies and turbulence set up by the hydraulic jump. The larger the hydraulic jump the greater the total head loss will be. This can be seen in figure 15 as the variation in the contraction ratio, between a gas with $\gamma = 2$ and water, increases as the Mach number increases. The variation across the oblique shocks (figure 14) is not as pronounced because the hydraulic jumps are smaller and do not vary as much with the Froude number.

2.5 Supersonic Perforated Intake Diffusers

The object of a supersonic intake diffuser, as used in air breathing engines, is to diffuse or compress a supersonic air stream. It is desirable for the diffuser to obtain maximum pressure recovery and mass flow recovery for efficient operation.

Supersonic-subsonic diffusion can easily be accomplished by having a shock ahead or at the inlet of the diffuser. However at high inlet Mach numbers the total pressure loss across the shock becomes prohibitive. The high pressure loss can be avoided by swallowing the shock in a convergent-divergent diffuser intake. However the throat area of a convergent-divergent diffuser must be larger to swallow a shock

than is necessary for isentropic diffusion at a design inlet Mach number (Refs. 12 and 13).

Diffusion must necessarily start from rest before design conditions are reached. The internal diffuser must therefore first swallow the shock before it can operate at its design Mach number. The shock may be swallowed in three ways. A maximum speed above the design speed could be used to swallow the shock or a variable geometry diffuser could be used to close down the throat area to isentropic design conditions after the shock was swallowed. However these two methods are not generally used because, in the first case the engine would operate at its maximum thrust only when swallowing the shock, and in the second case mechanical difficulties are involved. As a result, the shock is generally swallowed, in a convergent-divergent diffuser, by fixing the throat area to that required for swallowing the shock at the design inlet Mach number. Once the shock is swallowed the throat area will be larger than that required for isentropic diffusion at the design Mach number. The Mach number at the throat will therefore be greater than one and will increase through the divergent part of the diffuser after the throat. A strong shock will therefore occur some place downstream of the throat. The distance downstream of the throat will depend on the back pressure. A pressure loss will occur across the shock and the pressure recovery factor of the diffuser will be greater than that for isentropic diffusion with the shock occurring at the throat.

To overcome the starting difficulties of a supersonic convergent-divergent diffuser perforations can be placed in the converging part of the diffuser. The perforations have the same effect as that of increasing the throat area before the shock is swallowed. Thus the throat area can be designed for isentropic diffusion at a design Mach number and the shock can be swallowed by bleeding of air through the perforations until the isentropic design conditions are reached with the shock swallowed.

The perforations bleed off less air after the shock is swallowed because of pressure variations inside the diffuser. When the shock is at the inlet of the diffuser the static pressure in the supersonic portion is high compared to the pressure outside the diffuser and air will flow out of the perforations. As the shock moves towards the throat the pressure upstream of the shock in the diffuser becomes much lower and hence less mass flow will pass out through the perforations. The perforations act like automatic shut off valves as the shock passes them.

The placing of the perforations is important. The area distribution of the perforations and the diffuser cross-sectional area have been theoretically treated as a function of the Mach number in the diffuser by Eppard and Brown (Refs. 1 and 2). Perforations near the throat of the diffuser will have the greatest effect in swallowing the shock but are the least satisfactory as a shut off valve.

When the shock is just at the intake of the diffuser the pressure difference between the inside and the outside will be greatest at the perforations nearest the intake. Thus the greatest perforation spillage will occur through perforations near the intake. When the shock is swallowed the reverse is true and the perforation spillage through perforations nearest the intake will be the least. It is therefore true that the perforations near the intake act as the best shut off valves. This is desirable in order to obtain isentropic diffusion conditions with the greatest mass flow recovery factor. However the perforations near the intake will have an adverse effect in swallowing the shock once it has passed by shutting of the bleed off mass flow. Because of this the perforations should be close to the throat.

In the development of the theory for the perforated diffuser it was assumed that the area contraction ratio necessary for swallowing the shock was the same for the shock just at the inlet or swallowed. This is true for a convergent-divergent diffuser. Once the shock just starts to move towards the throat an unstable condition will cause the shock to move through the throat. This unstable condition is due to the total pressure loss across the shock decreasing with the decreasing Mach number obtained as the shock moves towards the throat. For a perforated diffuser this unstable condition is not necessarily set up because of the automatic shut off action of the perforations. However for perforations very near the throat it is reasonable to

assume that the contraction ratio will be the same for swallowing the shock whether it is at the inlet or near the throat.

A relationship between; the area contraction ratio ($\frac{A_1}{A_2}$), the inlet Mach number (M) and the mass flow recovery factor (X) for swallowing the shock can now be derived for a perforated diffuser with the perforations near the throat. Referring to figure (2a) and applying the continuity equation,

$$m_1 = m_p + m_2 \quad (46)$$

The mass flow recovery factor is

$$X = \frac{m_2}{m_1} = 1 - \frac{m_p}{m_1} \quad (47)$$

From non-dimensional mass flow relations

$$\frac{m_2 \sqrt{T_0}}{A_2 p_{0y}} = \frac{X m_1 \sqrt{T_0}}{A_2 p_{0y}} = f(M_{2y}) \quad (48)$$

and
$$\frac{m_1 \sqrt{T_0}}{A_1 p_{0x}} = f(M_{1x}) \quad (49)$$

dividing equation (48) by (49)

$$\frac{A_1}{A_2} = \frac{1}{X} \left(\frac{p_{0y}}{p_{0x}} \right) \frac{f(M_{2y})}{f(M_{1x})} \quad (50)$$

but when the shock is at the inlet of the diffuser

$$f(M_{2y}) = f(1) \quad (51)$$

$$\text{and } \frac{A_1}{A_2} = \left(\frac{1}{1 - \frac{m_p}{m_1}} \right) \left(\frac{p_{O_y}}{p_{O_x}} \right) \left(\frac{f(1)}{f(M_{1X})} \right) \quad (52)$$

$\frac{p_{O_y}}{p_{O_x}}$ can be determined as a function of M_{1X} from equation (45)

and $\left(\frac{f(1)}{f(M_{1X})} \right)$ can be determined from equation (44). The

theoretical relation between the three parameters: M_{1X} , A_1/A_2 , and X were plotted in figures 16 and 17 for an ideal gas with $\gamma = 1.4$.

3 DESCRIPTION OF APPARATUS AND TEST PROCEDURE

3.1 Apparatus

The apparatus was constructed at McGill University by the author. Pictures of the apparatus are shown in figures 3, 4 and 5. A scale isometric drawing is given in the appendix. The channel is supported at three points which are fixed in a frame constructed of 3" x 1 1/2" Dexion. Attached to the frame are two adjustable 5/8" diameter steel rods which support the height measuring carriage. The water flows from the channel through a collecting tank and storage tank and then is pumped back through a 1" diameter pipe to the stilling section of the channel as shown in figure 3.

The channel bottom was made from 1/2 inch plate glass. This was fitted into two 1/2 inch grooves machined into 1/2 inch plastic to form the channel walls. Strips of neoprene were placed in the grooves and the channel walls pressed to the channel bottom with tie rods. The joints were made water tight by sealing the underside of the glass to the plastic with an epoxy resin. The water entered the channel through a 3/8" slot in the back wall. A piece of neoprene was glued to the end of the channel to direct the flow into the 5 gallon collecting tank.

Two 8 1/2 x 1/2 inch pieces of 1/8 inch thick aluminium were fastened to the glass bottom with two sheets of neoprene in between. These two pieces of aluminium rested on the three supporting screws. Bending of the glass in the

longitudinal direction was prevented by proper placement of the supports, and by the grooves in the plastic walls. Bending of the glass across a section was held to a minimum by extending the aluminium plates across the channel.

Dexion was used for the frame for ease of construction. The $5/8$ inch diameter rods used to support the height measuring carriage were fastened by six adjustable screws and nuts to two lengths of angle iron, which were fixed to the frame. This allowed for fine adjustment of the carriage supports.

The carriage itself was made of two welded angle iron frames. The large frame moved along the fixed steel rods in the longitudinal direction. The smaller frame rested on the larger one and was free to move in a direction across the channel. A rectangular piece of iron was attached to the centre of the smaller frame. This held a micrometer fixed in the vertical position. A needle was attached to the end of the micrometer. Scales were attached along and across the channel. Thus vertical heights at any position in the test section and stilling section could be measured and their position recorded.

A Southern "58" circulator pump, 1 inch size, was used to circulate the water (figure 3). Operating at a head of three feet the pump delivered 25 U.S. gallons per minute. The size of the pump was calculated to give a flow corresponding to a simulated Froude number of 3 for the given channel, with

a water depth of about $1/4$ of an inch. The limitation of a $1/4$ inch water depth greatly reduced the amount of flow required. The flow of water was controlled by a one inch gate valve placed just before the channel inlet. A $1/4$ inch by-pass valve was installed to give finer flow adjustment. In order to maintain a more constant height in the stilling section, a 20 gallon storage tank was placed after the collecting tank.

A conventional de Laval shaped nozzle was not used to obtain shooting flow in the test section of the channel. Instead a gate across the channel was used to separate the test section from the stilling section. This type of sluice nozzle (figures 1 and 5) eliminated the cross flow inherent in the de Laval type. The velocity of water flow was easily varied in the test section by varying the height in the stilling section. Two difficulties were encountered with the sluice nozzle. Waves initiating from the corners of the gate could only partially be eliminated by forming plasticene side walls upstream of the sluice nozzle. The difficulty was completely eliminated by placing the diffuser inlet inside the hydraulic jumps initiating from the corners (figure 5). The second difficulty was to obtain a smooth under surface of the sluice nozzle with a sharp edged outlet. The sluice nozzle was machined from plastic and a satisfactory surface was obtained with rouge paper.

The diffuser model was made of plastic (figure 5). The converging portion is 3.8 inches long and the diverging portion approximately 4 inches. The intake of the diffuser was machined as a straight wedge at an angle of 4 degrees. A one degree slope was made in the diverging portion. Two $3/8$ inch diameter holes were drilled side by side, at an angle to the wedge, just before the throat in order to simulate a perforated diffuser. The two holes on each side were smoothed out and plasticene was used to give a uniform slit $1/4$ of an inch by $1/2$ of an inch close to the channel bottom. The slits were connected to moulded plastic tubes on the outside of the diffuser. Rubber hoses were fastened to the tubes and led to a bucket below the working section (figure 3). The water flow siphoned off through the perforations was adjusted with a clamp placed around the rubber tubes. The two sides of the diffuser were held in place on the channel bottom by pressure from two moveable plastic arms. (figure 5) The area contraction ratio of the diffuser could therefore be easily altered.

The 20° wedge model (figure 5), which was used to determine oblique shock angles, was made of plastic. It is approximately $1/2$ an inch high and 2 inches long.

The supersonic water pitot was machined from brass (figure 5). It is approximately 2.5 inches high with a $1/2$ " hole drilled through the centre in the vertical direction. This area inside acts as a stilling

section for the flow which enters through a $1/8$ inch slit. Fluctuations of the stagnation height in the stilling section were reduced by inserting a plug in the upper portion of the inlet slit.

Smooth flow was obtained in the stilling section by passing the water through two wire mesh screens and an upstream sluice. The amount of screens, to smooth the flow, was limited by the capacity of the pump.

3.2 Test Procedure

The water channel was calibrated before the tests were carried out on the supersonic diffuser model. Before any readings were taken the channel floor was first levelled by means of the three adjusting screws. The height measuring carriage was then levelled by taking readings on the glass bottom at positions: A, B, C and D (figure 1a) and adjusting the two carriage rods. The water was then allowed to flow down the channel and the positions of the gate valve and by-pass valve recorded. The sluice nozzle was adjusted to give an outlet water depth of approximately $1/4$ of an inch. The channel was then inclined so that the hydraulic jump just moved off the end of the test section a distance of about $2 \frac{1}{2}$ channel widths from the sluice nozzle. The slope was recorded.

For the first few tests the temperature of the water was recorded but the temperature variations observed had

a negligible effect on the density. The density of the water was taken to be constant at 62.4 lbs./ft.³

The channel was allowed to operate for at least 15 minutes before any readings were taken in order to obtain steady conditions. When the flow became steady the water depths were measured at the positions h_1 , h_2 , h_3 , h_4 , h_5 and h_0 (figure 2). From these measurements h/h_0 , A_c and A_{0c} were obtained, knowing the width of the channel. The slope was also obtained by recording the height of the channel bottom at positions h_0 and h_{14} .

The wedge was then placed in the channel and the oblique shock angle measured with a protractor.

The supersonic water pitot was placed in the channel and the water depths and h_0' , h_x and h_y were measured. h_x/h_0' was then determined.

The diffuser was then placed in the channel and the area contraction ratio determined experimentally for a 100% mass flow recovery factor. This was determined by opening up the diffuser until the hydraulic jump just moved down through the throat from the inlet. Little difference was found in the contraction ratio for the hydraulic jump at the inlet of the diffuser and the hydraulic jump just swallowed. The widths of the diffuser were measured at the throat and inlet with dividers and a scale.

Finally the mass flow through the whole apparatus was measured by diverting the water into a bucket

just before the storage tank. The time required to fill the bucket was recorded and the bucket weighed.

The above measurements were recorded at nine different mass flows and the calibration curves obtained. (figures 11, 12, 13 and 14) These curves are discussed in section 3.3.

The perforated diffuser was tested at five different mass flow recovery factors for each of seven different Froude numbers. The test positions were obtained by first setting the hydraulic analogue at an approximate mass flow. The perforation spillage was then set at approximate mass flows by sight judgement of the flow from the spillage tube.

The perforation mass flow was measured by collecting the water from the spillage tube for a recorded time interval of not less than five minutes. The water was weighed and m_p calculated. The diffuser was then opened, with the same perforation spillage, until the hydraulic jump was just swallowed. The outsides of the diffuser were kept parallel so that the diffusion angle remained constant at approximately 4° . The diffuser widths at the throat and inlet were measured and the water heights at the positions h and h_o were recorded. The perforation spillage was then changed and the procedure repeated.

The Froude number was obtained from the ratio h/h_0 , and the calibration curve, figure 11. The value of $m/A\sqrt{h}$ was then obtained from the Froude number and the calibration curve (figure 13). The mass flow through the diffuser inlet was calculated from the equation,

$$\left(\frac{m}{A\sqrt{h}}\right) A_1(h)^{1.5} = m_\phi \quad (53)$$

From m_ϕ and m_p the mass flow recovery factor was calculated from equation (47).

The contraction ratio (W_1/W_2) was calculated from direct measurement of the two-dimensional diffuser widths at the inlet and the throat.

A second method was used to determine experimentally the relationship between the contraction ratio, the inlet Froude number and the mass flow recovery factor necessary for swallowing an hydraulic jump. This was done as a check on the results obtained at simulated isentropic conditions. Instead of fixing the Froude number and the perforation spillage and then varying the contraction ratio to swallow the hydraulic jump, the contraction ratio was set at the simulated isentropic contraction ratio for a fixed Froude number and the perforation spillage increased until the hydraulic jump was swallowed. The simulated isentropic choking conditions were also obtained by reducing the perforation spillage after the hydraulic jump was swallowed.

All the photographs of the flow patterns were obtained with a Samoca 35 mm. camera supported on a tripod placed above the apparatus. Kodak plus X film was used. The film was developed in C-2 Uni bath to give an exposure index of 400 A.S.A. Most of the photographs were taken at $1/300$ of a second at $f 16$ and a camera to object distance of 3.5 feet.

Photographs of the water surface waves in the simulated perforated diffuser were obtained by two different techniques (figure 6). Photographs of the surface waves can be obtained by reflecting light from the water surface, or by obtaining an image of the refracted light passing through the water surface, from a source below the glass bottom of the channel, and on to a frosted glass plate just above the model. Both these methods are described by B. Langtrej (Ref. 9).

3.3 Calibration of the Hydraulic Analogue

The Froude number can be determined experimentally by five different methods. The parameters h/h_0 , h_x/h_0' , $m/A \sqrt{h}$, β and W_1/W_2 were experimentally determined as indicated in section 3.2. From each of these values the Froude number can be determined using the theoretical curves (figures 11 to 15) derived in section 2.2. The experimental Froude numbers obtained from each of the above parameters should be the same.

For convenience the Froude number obtained from the measured values of h/h_0 was used as a reference value and the experimental values of h_x/h_0' , $m/A \sqrt{h}$, β , and W_1/W_2 were plotted against this reference Froude number (figures 12 to 15). It can be seen that in each case the experimental curves did not agree with the theoretical curves for water. In other words, the Froude number obtained from h/h_0 does not agree with the Froude numbers that would be obtained from any of the other parameters.

The Froude number obtained from the experimental values of h_x/h_0' was then used to plot a second set of experimental curves (figures 11 and 13 to 15). A greater disagreement was found for the Froude numbers obtained from h_x/h_0' than from the Froude numbers obtained from h/h_0 with the theoretical Froude numbers for $m/A \sqrt{h}$ and W_1/W_2 . However the Froude numbers obtained from the measured values of h_x/h_0' and β agree closely (figure 14).

The disagreement between the Froude numbers obtained from the parameters h/h_0 , h_x/h_0' , $m/A\sqrt{h}$, and W_1/W_2 could be caused by experimental error or deviations between the actual water flow, and the theoretical water flow. The experimental error in measuring the water depths with the micrometer was within $\pm .005$ inches. This would result in a maximum experimental error in the Froude number, obtained from h/h_0 and h_x/h_0' of $\pm .05$. The error in measuring the oblique shock angle was ± 1 degree, the widths of the diffuser were measured to within $\pm .02$ ". This would give an average experimental error of $\pm .03$ for the contraction ratio W_1/W_2 . The mass flow parameter ($m/A\sqrt{h}$) error was undetermined but from consideration of the short time interval of 20 seconds, which was used to calculate m , the experimental error could be very large. It was also noticed that the flow conditions changed during the time interval for measuring m . This was particularly noticeable at the higher mass flows. From the above considerations and because the differences in the Froude number were not of a random nature (figures 11 to 15) it was concluded that the differences in the Froude number were not due to experimental error.

In order to obtain the most correct value of the Froude number, an examination of the theoretical relations used to determine the Froude number from the experimental values was made. It was first assumed that the Froude number obtained from the measured values of h/h_0' was the most

correct one because it agreed closely with the Froude number obtained from β (figure 14). For this value to be correct, the theoretical values of the Froude number obtained from h/h_0 and W_1/W_2 must be too low, particularly at the higher Froude number (figures 11 and 15). In the derivation of the relations between F and h/h_0 and between F and W_1/W_2 it was assumed that there was no loss of energy between h and h_0 and between W_1 and W_2 . From a re-arrangement of equation 16

$$F^2 = 2 \left(\frac{h_0}{h} - 1 \right) \quad (16a)$$

An examination of equation 16a shows that if there is a loss of energy between h_0 and h , h will be theoretically larger than the experimental values of h and will result in a lower value for the Froude number. It can similarly be shown that the theoretical value obtained for the Froude number from W_1/W_2 will be smaller than the experimental value if there is a loss of energy between W_1 and W_2 . It would appear therefore that the loss of energy would account for the discrepancy between the theoretical curves, and the experimental curves obtained from the relation between h_x/h_0' (F) and W_1/W_2 and between h_x/h_0' (F) and h/h_0 . The deviations would be larger at the higher Froude numbers because the loss of energy would be greater.

It should be noted that the energy was also assumed constant for the relation between h_x/h_0' and F .

However the distances over which the energy was assumed constant were less between h_x and h_o' than between h and h_o and between W_1 and W_2 . The distance between W_1 and W_2 over which the energy was assumed constant was the greatest distance and hence the largest difference between the theoretical and experimental values was obtained. Because the energy between h_x and h_o' was assumed constant it was concluded that the true Froude number would be somewhat less than the Froude number obtained from h_x/h_o' . The Froude number obtained from h_x/h_o' was concluded to be the most accurate.

The experimental results obtained for $m/A \sqrt{h}$ were not considered because of the experimental error involved. However the above considerations could be applied.

4. DISCUSSION AND RESULTS

The results obtained from the tests carried out on the supersonic perforated diffuser in water are shown in figure 16. The contraction ratios were plotted against the mass flow recovery factors for various inlet Froude numbers, based on the values of h/h_0' , required to swallow an hydraulic jump. Constant Froude number curves were drawn. The variations between the test points and the smooth curves were within the experimental error (section 3.3). From these curves the experimental carpet graph was plotted as shown in figure 17.

The theoretical relation between the contraction ratio, the mass flow recovery factor and the inlet Mach number, required to swallow a shock for an ideal gas with $\gamma = 1.4$, was also plotted in figures 16 and 17. From figure 17 it can be seen that for mass flow recovery factors above 85% there is good agreement between the theoretical values and the experimental values. However for mass flow recovery factors below 85% the experimental contraction ratios are smaller than the theoretical contraction ratios for a constant inlet Mach number or Froude number. In effect, a larger throat width was required experimentally to swallow an hydraulic jump at the larger perforation mass flows than was theoretically required to swallow a shock.

At the higher perforation mass flows there is a suction effect near the throat which would tend to decrease the effective throat width. Therefore a larger physical throat width would be required to swallow the hydraulic jump. This suction effect would cause the deviations of the experimental results from the theoretical results at the lower mass flow recovery factors.

It was mentioned that the simulated Mach number, or Froude number, used in plotting the experimental results in figures 16 and 17 was obtained from the measured values of h and h_0 . This Froude number was not the true Froude number for the hydraulic analogy (section 3.3). The Froude number obtained from the measured values of h_x and h_0' would be more correct. However it can be seen from figure 15 that the Froude number obtained from h_x/h_0' was uniformly higher than that obtained from h/h_0 . Therefore the effect of using the more correct Froude number obtained from h_x/h_0' would be to shift the experimental carpet plot (figure 17) to the right. The experimental results would not compare to the theoretical results absolutely, however the relative experimental results would still compare closely to the relative theoretical results.

In the derivation for the theoretical gas curves shown in figures 16 and 17 it was assumed that the contraction ratio, necessary for swallowing a shock in a diffuser with perforations near the throat, was the same as

that for the shock just at the inlet of the diffuser (section 2.5). This assumption was found to be true for the experimental perforated water diffuser with the perforations near the throat. Once the hydraulic jump just started to move down the throat it was swallowed.

The experimental test points, obtained by setting the diffuser contraction ratio at isentropic conditions for the given simulated Mach number and increasing the perforation spillage until the hydraulic jump was swallowed, were found to agree with the other experimental results. The perforation bleed off for choking the diffuser, at an isentropic contraction ratio for the simulated Mach number, was obtained at three points. The maximum inlet simulated Mach number was limited, by the mass flow bleed off, to 1.7. The results were inconclusive and were not plotted.

The photographs of the surface waves shown in figures 7 to 10 were all obtained using light refraction, or the shadowgraph technique. This technique requires parallel light to pass through the water surface. Parallel light was not obtained from the light source available therefore the photographs of the wave patterns were distorted. However the distortion was negligible as the light rays were almost parallel.

Figures 6a and 6b show the hydraulic jump at the intake of the diffuser. The three dimensional effect obtained by reflecting the light from the surface can be seen in figure 6a.

Figure 7a shows clearly the characteristic oblique shocks obtained in supersonic gas flows. They are simulated by the gravity waves in the water shown as dark bands. The smaller waves have no part in the hydraulic analogy. They are capillary waves. A simulated shock intersection is shown where the two oblique gravity waves meet in the middle of the diffuser. The upstream included angle where the gravity waves meet is not equal to the downstream included angle which is the case for oblique shock intersections.

Figure 7b shows the flow pattern in the diffuser with a perforation mass flow and the hydraulic jump at the inlet. The water flow simulates a strong shock near the intake of the diffuser with the characteristic lambda configuration. The relatively straight parallel lines just after the throat of the diffuser indicate a series of weak normal shocks. This supersonic condition after the throat was a result of the high perforation bleed off. The small disturbances upstream of the diffuser were caused by very small bumps or grooves at the exit of the sluice nozzle. The disturbances issuing from the top and bottom were from the corners of the diffuser.

Figure 8 shows a characteristic bow wave simulated by the curved gravity wave in front of the diffuser. The smooth flow inside the diffuser would indicate subsonic conditions.

Figure 9 illustrates the difference in the contraction ratio required to swallow an hydraulic jump with and without mass flow bleed off.

Figure 10 shows the hydraulic jump being swallowed as the Mach number was increased.

The water surface wave patterns (figures 6 to 10) were found to exhibit the same configurations as found in supersonic gas flows. It should be noted that the simulated Mach numbers for the photographs were based on the Froude number that would be obtained from a Supersonic Water Pitot.

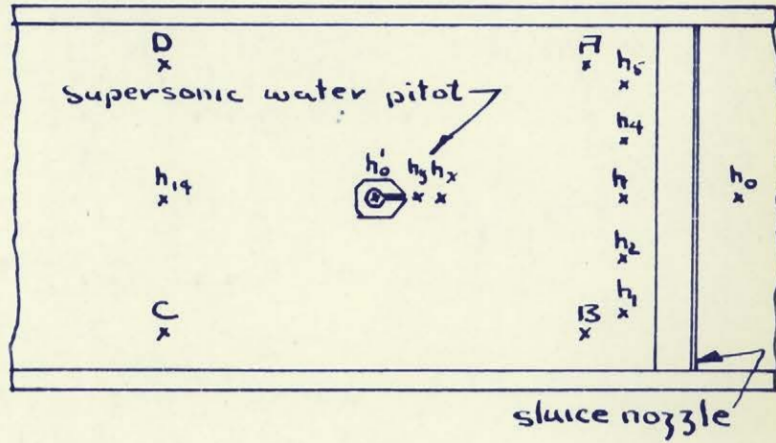
5. CONCLUSIONS

1. The Froude number could not be obtained accurately.
2. The supersonic water pitot was the most accurate method to determine the Froude number.
3. The experimental results obtained from the perforated diffuser model agreed closely with the theoretical relations developed for a gas, with a specific heat ratio of 1.4, at mass flow recovery factors above 85%. The agreement was due to a fortuitous choice of obtaining the Froude number.
4. The contraction ratio required for swallowing an hydraulic jump in a perforated diffuser, with the perforations near the throat, was almost the same as that required when the hydraulic jump was near the intake.
5. Quantitative results obtained from the hydraulic analogue cannot be applied to supersonic gas flows.
6. The hydraulic analogue is a good apparatus for studying supersonic flows qualitatively in a supersonic diffuser.

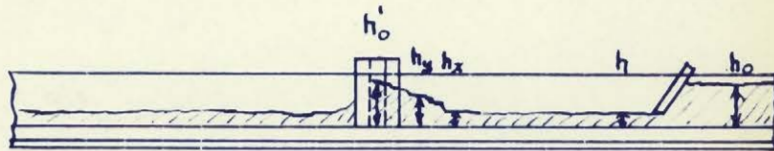
REFERENCES

1. Evvard, J.C. and Blakey J.W.
"The Use of Perforated Inlets for Efficient Supersonic Diffusion"
N.A.C.A. T.N. 3767 Sept. 1956.
2. Brown, D.
"An Experimental Investigation of the Pressure Recovery of a Perforated-Wall Internal-Compression Intake at a Free-Stream Mach Number of 2.5"
Institute of Aerophysics, University of Toronto
T.N. No. 18 May 1957.
3. Clark, J.P.C.
"An Experimental Investigation of a Supersonic Two-Dimensional Perforated Inlet of a Nominal Free Stream Mach Number of 2.5"
Institute of Aerophysics, University of Toronto
UTIA Tech. Note No. 24 Nov. 1958.
4. Preiswerk, E.
"An Application of the Methods of Gas Dynamics to Water Flow with Free Surface"
I. Flows With no Energy Dissipation.
II. Flows With Momentum Discontinuities.
N.A.C.A. T.M. 934 and 935 1940.
5. Shapiro, A.H.
"An Appraisal of the Hydraulic Analogue to the Gas Dynamics"
Meteor Report No. 34 MIT April 1949.
6. Crossley H. E. Jr.,
"The Analogy Between Surface Shock Waves in a Liquid and Shocks in Compressible Gases"
Cal. Institute of Tech., Hydrodynamics Laboratory,
Report No. N-54.1 Aug. 1949.
7. Supino, G.
"Air-Water Analogy and the Study of Hydraulic Models"
N.A.C.A. T.M. 1359 July 1953.

8. Orlin W.J., Lindner, N.J. and Bitterly J.G.
"Application of the Analogy Between Water Flow with
a Free Surface and Two-Dimensional Compressible Gas
Flow"
N.A.C.A. Report No. 875, 1947.
9. Langtry, B.D.
"A Study of Supersonic Diffusers; an Application of the
Hydraulic Analogy"
Thesis (S.M.) M.I.T. 1948.
10. Goldman, K. and Meerbaum, S.
"Hydraulic Analogy of Supersonic Flow"
Thesis (S.M.) M.I.T. 1946.
11. Milne-Thomson, L.M.
"Theoretical Hydrodynamics"
Macmillan 3rd Edition.
12. Shapiro, A.
"The Dynamics and Thermodynamics of Compressible Flow"
Ronald Press, New York 1954.
13. Herman, R.
"Supersonic Inlet Diffusers and Introduction to Internal
Aerodynamics"
Minneapolis-Honeywell Regulator Co. Ltd.
Aeronautical Division. 1956.
14. Lamb, H.
"Hydrodynamics"
6th Ed. Dover Publications 1945.
15. Wu, J.H.T.
"An Experimental Study of Perforated Intake Diffusers
at a Free Stream Mach No. of 2.50"
UTIA Report (to be published).
16. Loh, W.H.T.
"Hydraulic Analogy for Two-Dimensional and One-Dimensional
Flows"
Journal of the Aero/Space Sciences
Vol. 26 No. 6. June 1959.



a. TOP VIEW OF TESTING SECTION



b. SIDE VIEW OF TESTING SECTION

FIGURE 1. LOCATION OF MEASURING POINTS.

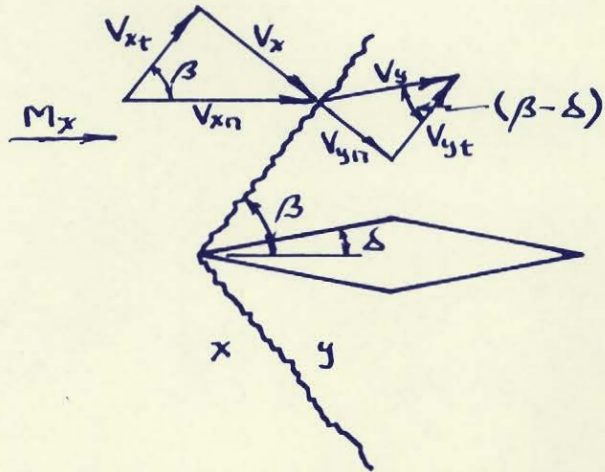


FIGURE 2a OBLIQUE SHOCK OR HYDRAULIC JUMP
FROM SUPERSONIC WEDGE

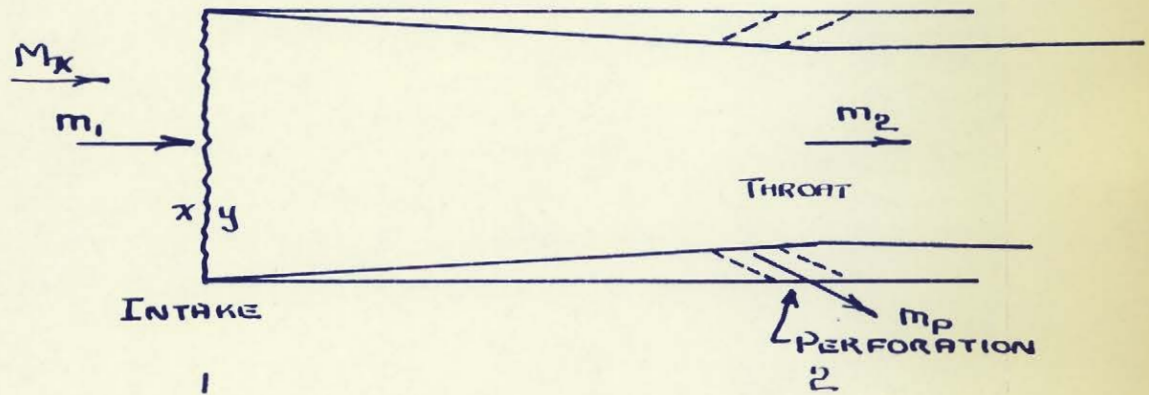


FIGURE 2b PERFORATED SUPERSONIC
DIFFUSER WITH A SHOCK OR
HYDRAULIC JUMP AT THE INTAKE

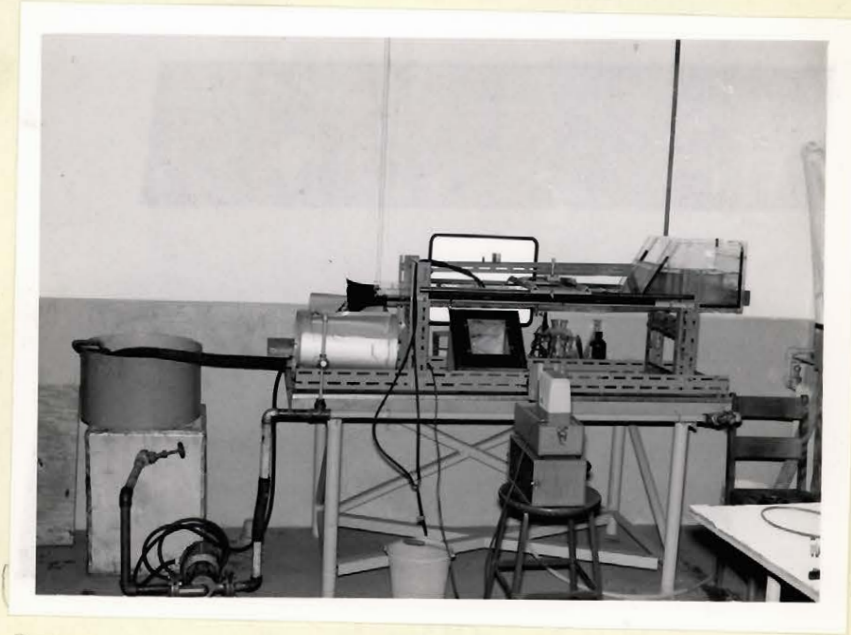


FIGURE 3 THE HYDRAULIC ANALOGUE

The side view of the apparatus shows the water channel supported in the dexion frame, the collecting tank, the storage tank, the pump and the flow pipes with the gate valve and by-pass. The perforation spillage tubes are shown leading from the testing section to the collecting bucket. The camera tripod was removed but the light source and the inclined mirror can be seen in position.

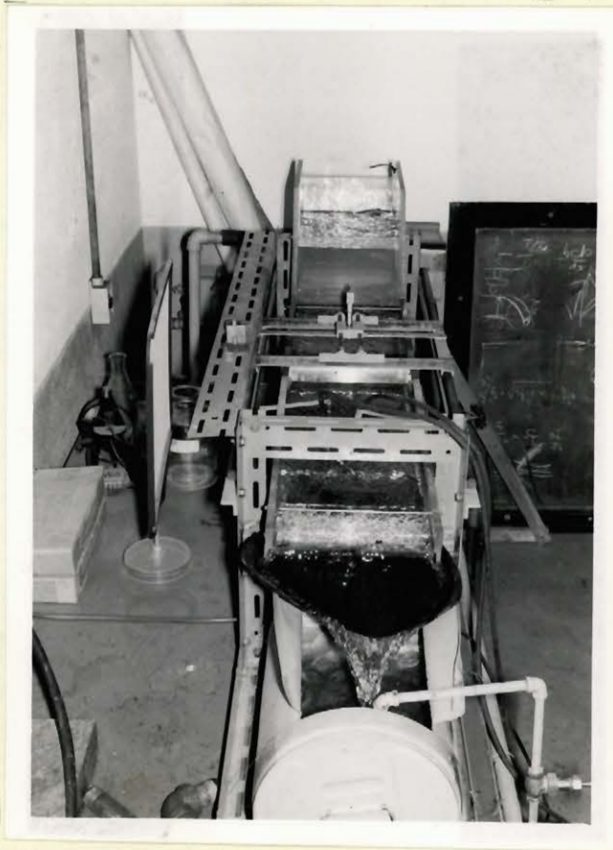


FIGURE 4 THE HYDRAULIC ANALOGUE

A view from the downstream end of the channel showing the testing section and the two stilling sections. The tie rods holding the side walls can be seen along the channel. The height measuring carriage is shown resting on the adjustable support rods.

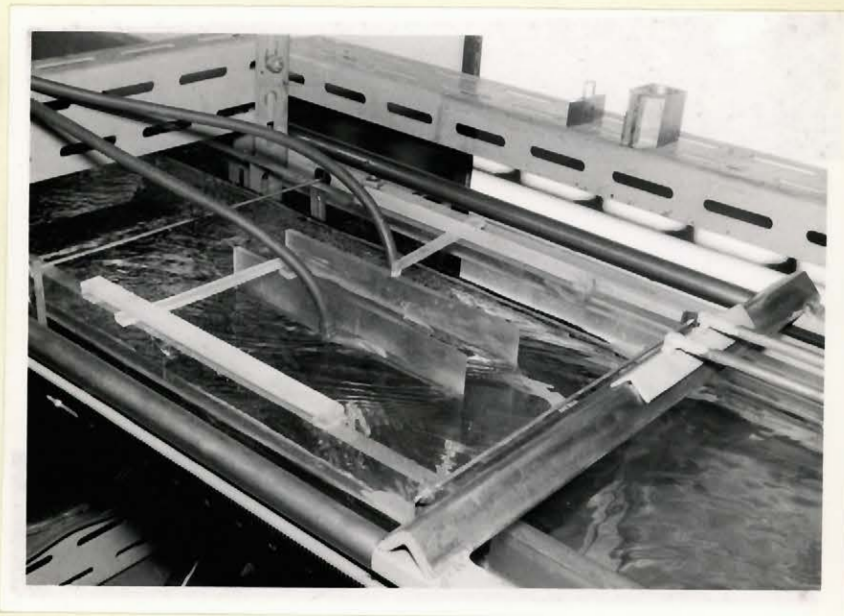
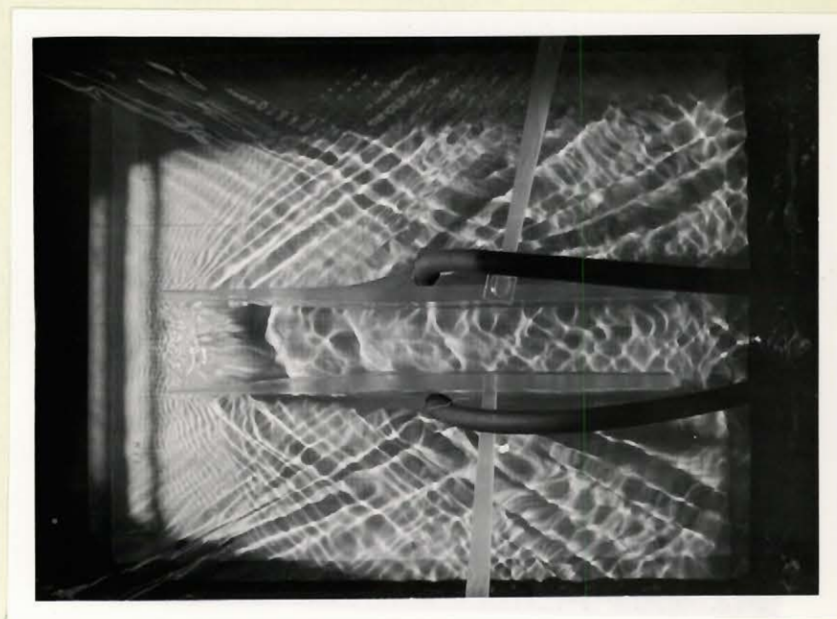


FIGURE 5 TESTING SECTION OF HYDRAULIC ANALOGUE

The testing section of the channel is shown with the supersonic perforated diffuser model held in place with the adjustable model holders. The top part of the sluice nozzle can be seen just above the measuring carriage. The supersonic water pitot and the 20° wedge are shown resting on the frame at the back. The inlet of the diffuser model is inside the waves issuing from the corners of the sluice nozzle.

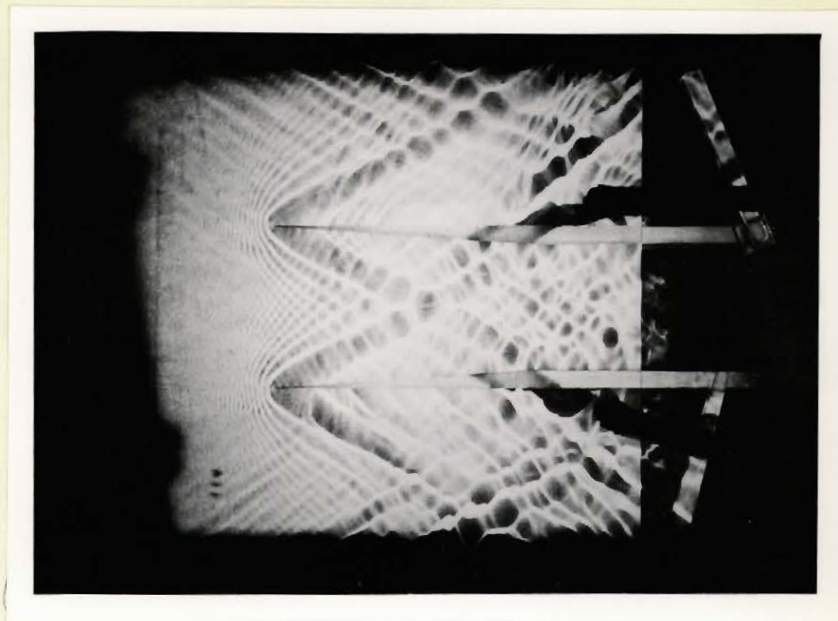


(a) Simulated Mach Number ≈ 2.4
Mass Flow Recovery Factor $\approx 100\%$
Contraction Ratio = 1.48

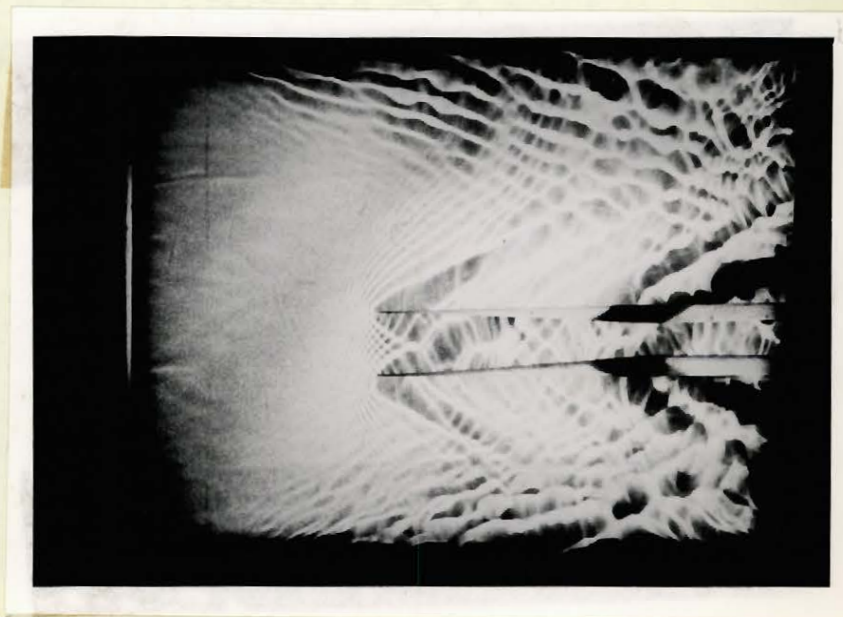


(b) Simulated Mach number ≈ 2.3
Mass Flow Recovery Factor $\approx 75\%$
Contraction Ratio = 1.76

FIGURE 6 Comparison between two methods of photographing surface waves; (a) by reflection of light, and (b) by the shadowgraph technique. The hydraulic jump is at the diffuser inlet in both cases.

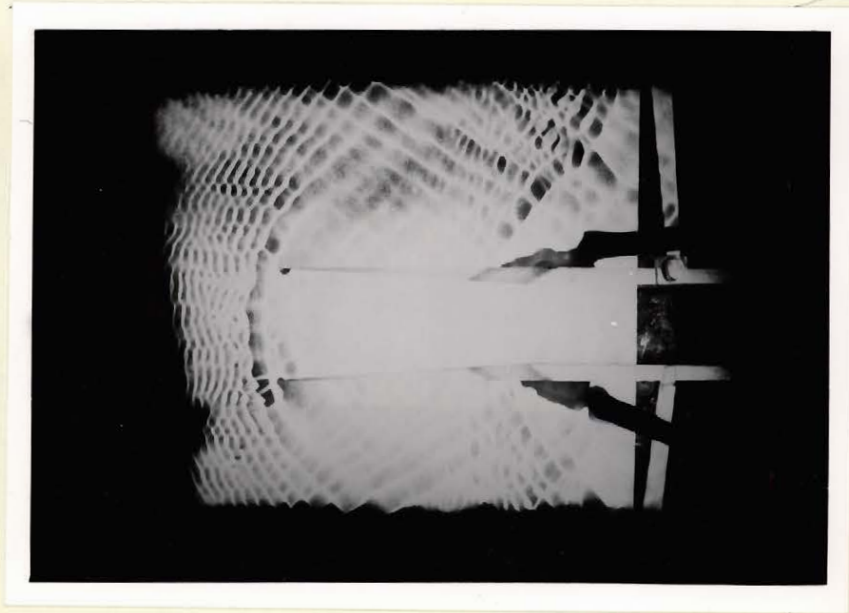


(a) Simulated Mach Number ≈ 2.9
Mass Flow Recovery Factor $\approx 100\%$
Contraction Ratio $= 1.32$
Hydraulic Jump Swallowed



(b) Simulated Mach Number ≈ 3.5
Mass Flow Recovery Factor $\approx 75\%$
Contraction Ratio $= 2.06$
Hydraulic Jump at the Intake.

FIGURE 7 FLOW PATTERNS IN A SUPERSONIC PERFORATED DIFFUSER WITH AND WITHOUT BLEED OFF



Simulated Mach Number ≈ 2.3
Mass Flow Recovery Factor = 100%
Contraction Ratio = 1.39

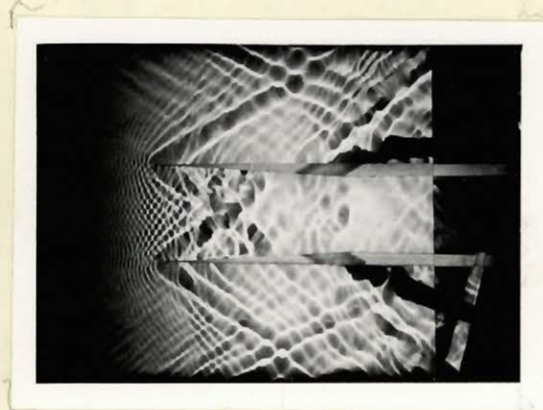
FIGURE 8 ILLUSTRATION OF BOW WAVE AT INLET TO
SUPERSONIC DIFFUSER.



(a) Contraction Ratio = 1.37



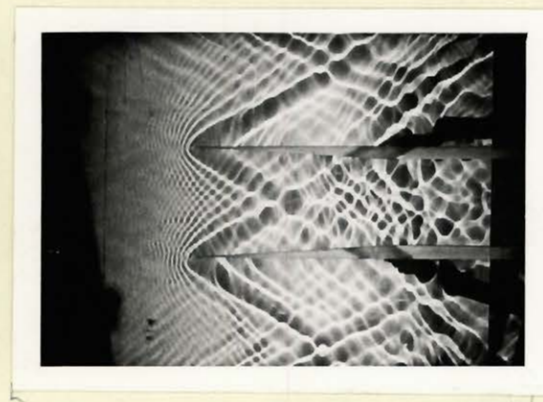
(d) Contraction Ratio = 1.67



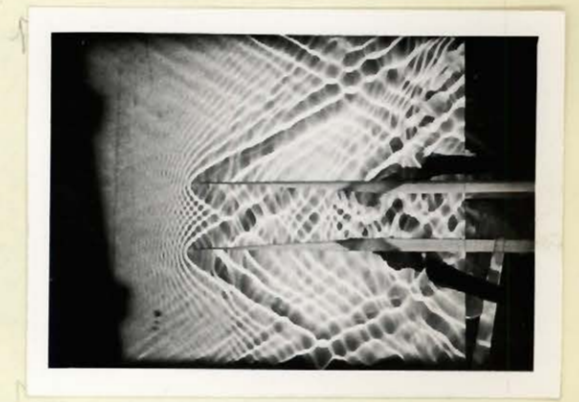
(b) Contraction Ratio = 1.35



(e) Contraction Ratio = 1.58

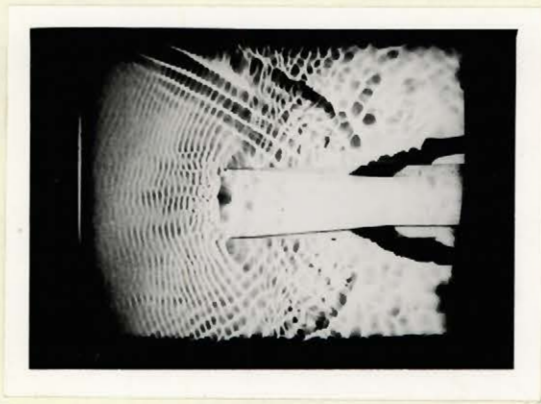


(c) Contraction Ratio = 1.30

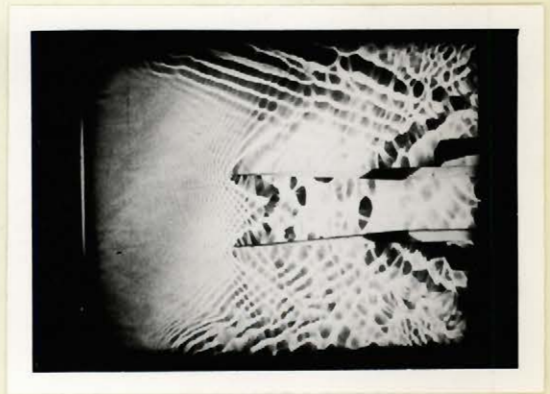


(f) Contraction Ratio = 1.48

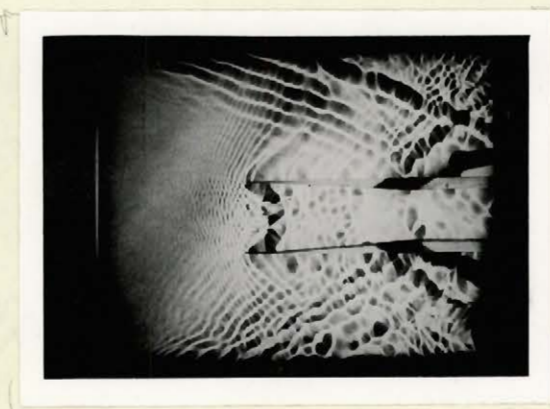
FIGURE 9. Comparison of Contraction Ratios required to swallow an Hydraulic Jump with a Mass Flow Recovery Factor = 100% (a, b, c) and a Mass Flow Recovery Factor $\approx 85\%$ (d, e, f). The simulated Mach number ≈ 2.8 for all the photographs. The Hydraulic Jump is Swallowed in c and f and in the process of being swallowed in b.



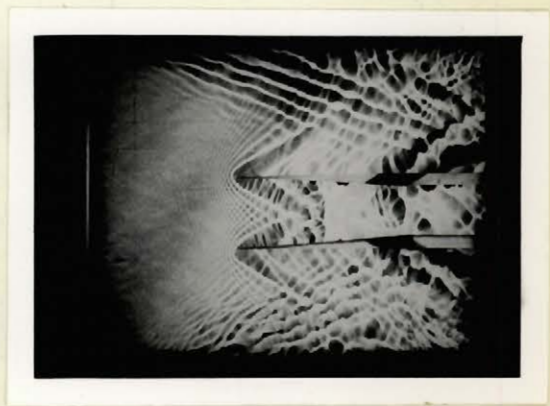
(a) M 1.9



(c) M 2.6

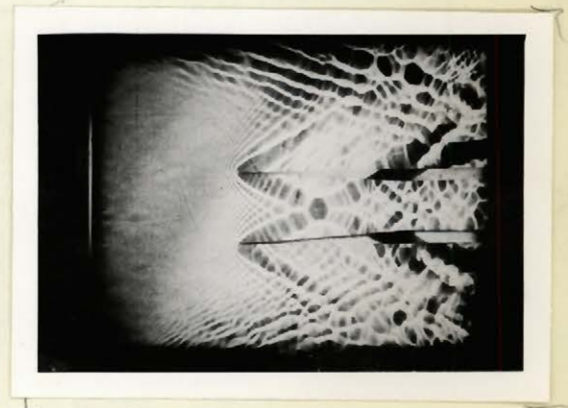


(b) M 2.2



(d) M 2.6

FIGURE 10 The different positions of the Hydraulic Jump in the Perforated diffuser model are shown in a and b as the inlet simulated Mach number increases; and in c, d, and e as the hydraulic jump is swallowed. The Area Contraction Ratio is constant and = 1.33. The Mass Flow Recovery factor is constant and $\approx 90\%$.



(e) M 2.6

HEIGHT RATIO ACROSS SLUICE NOZZLE
VS
FROUDE NUMBER

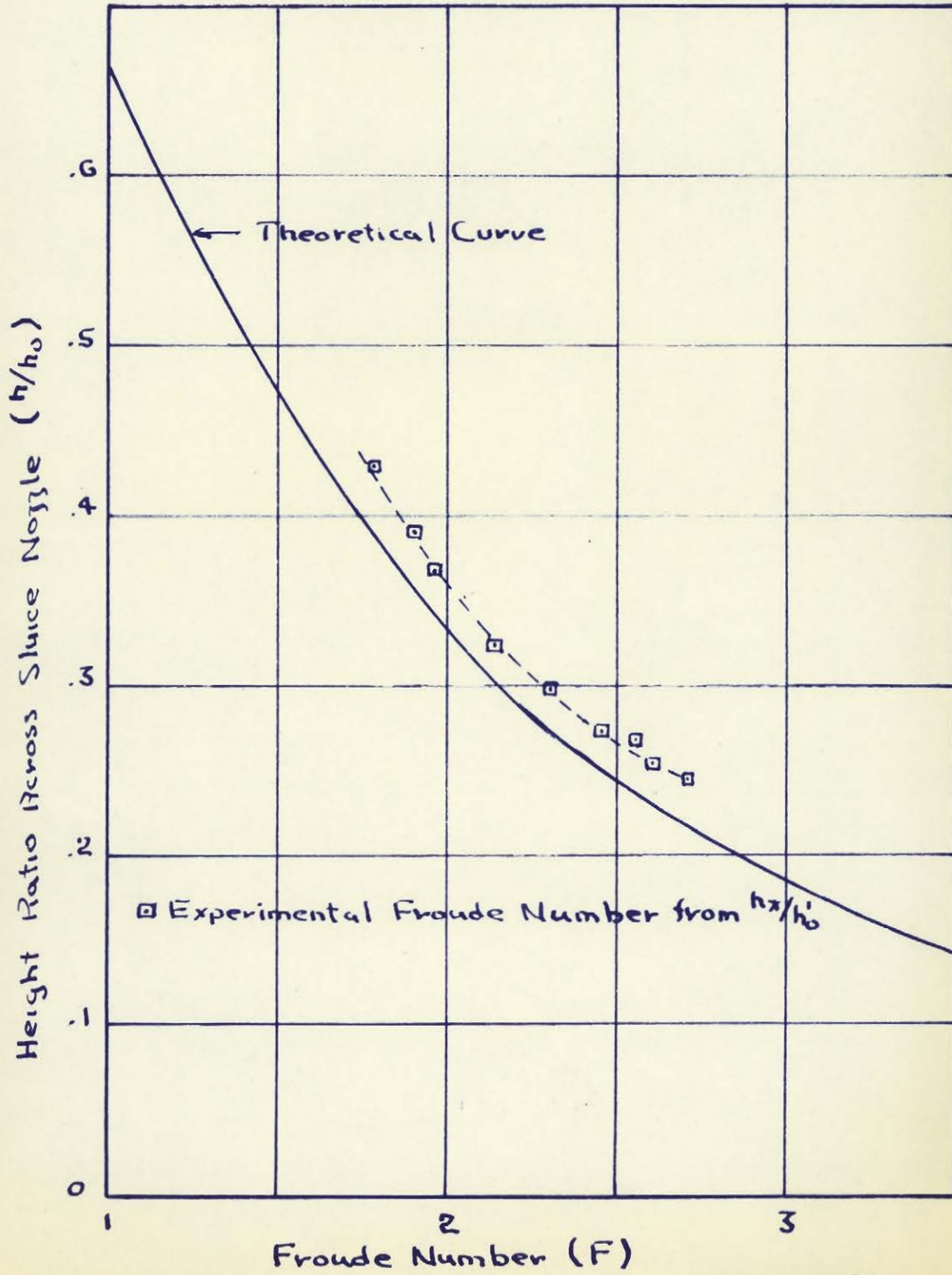


Figure 11

HEIGHT RATIO FOR SUPERSONIC WATER PITOT vs FROUDE NUMBER

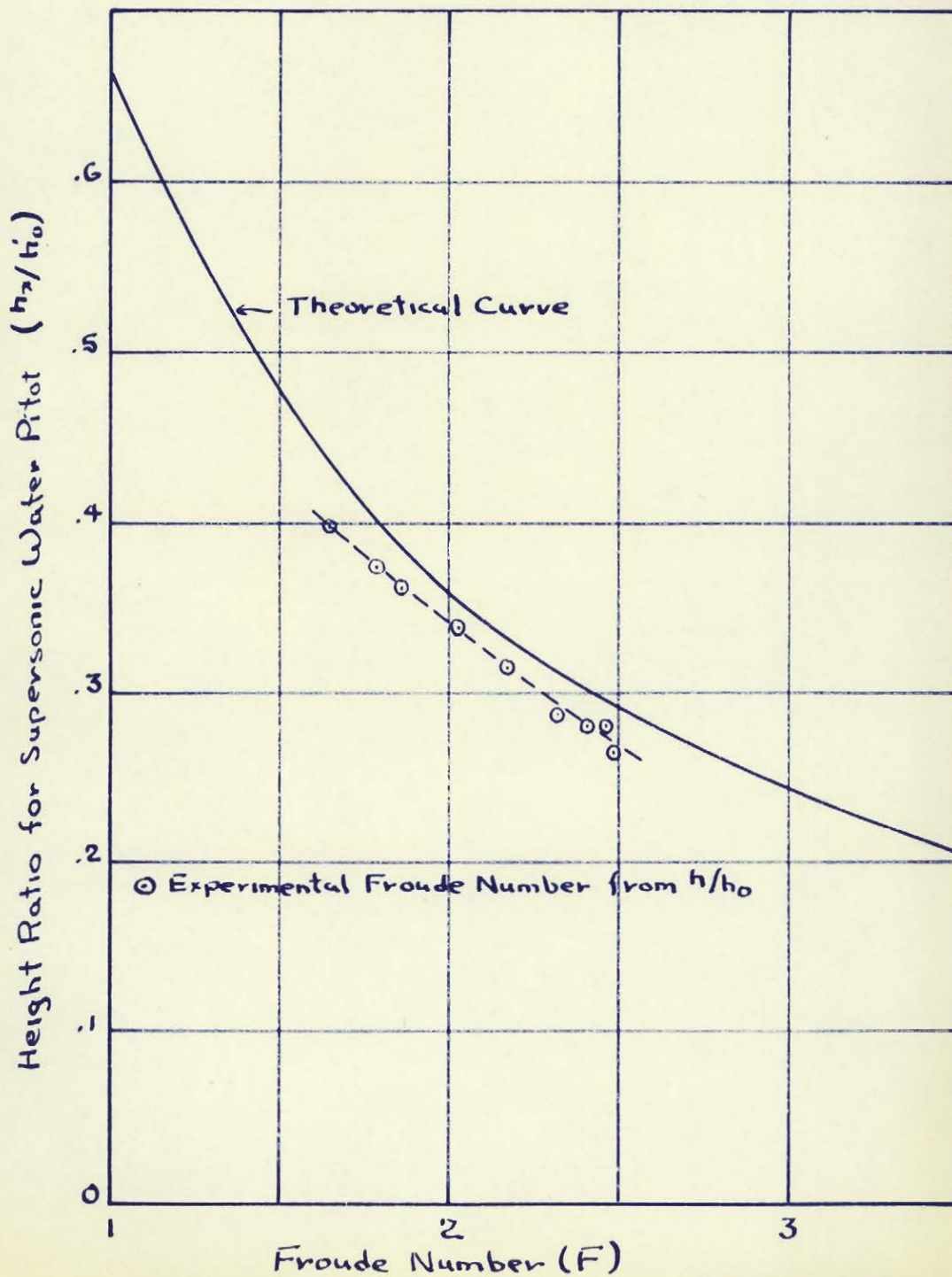


Figure 12

MASS FLOW RATIO
vs
FROUDE NUMBER

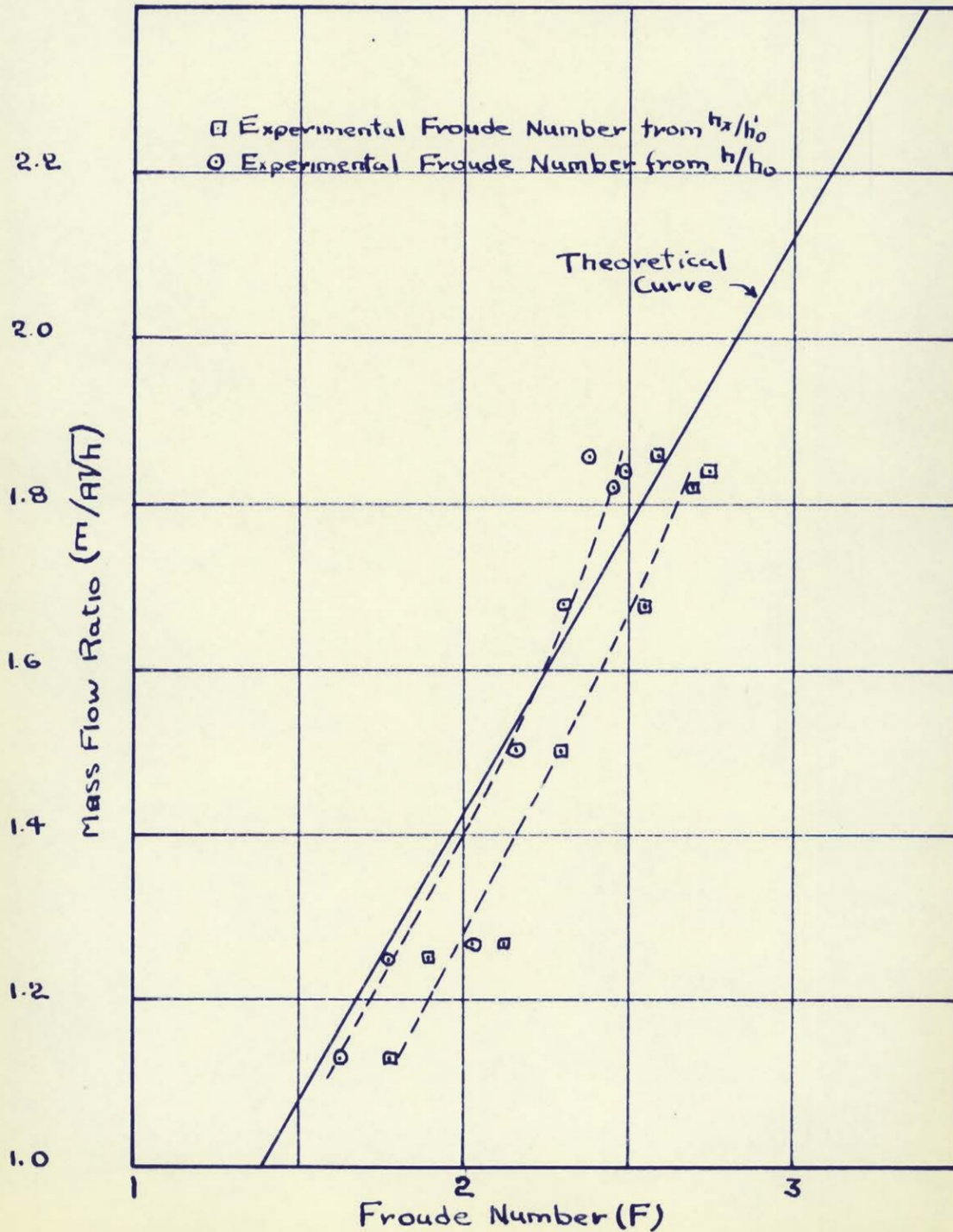


Figure 13

UPSTREAM FROUDE AND MACH NUMBERS
VS
OBLIQUE HYDRAULIC JUMP AND SHOCK ANGLES
FOR A 10° WEDGE ANGLE

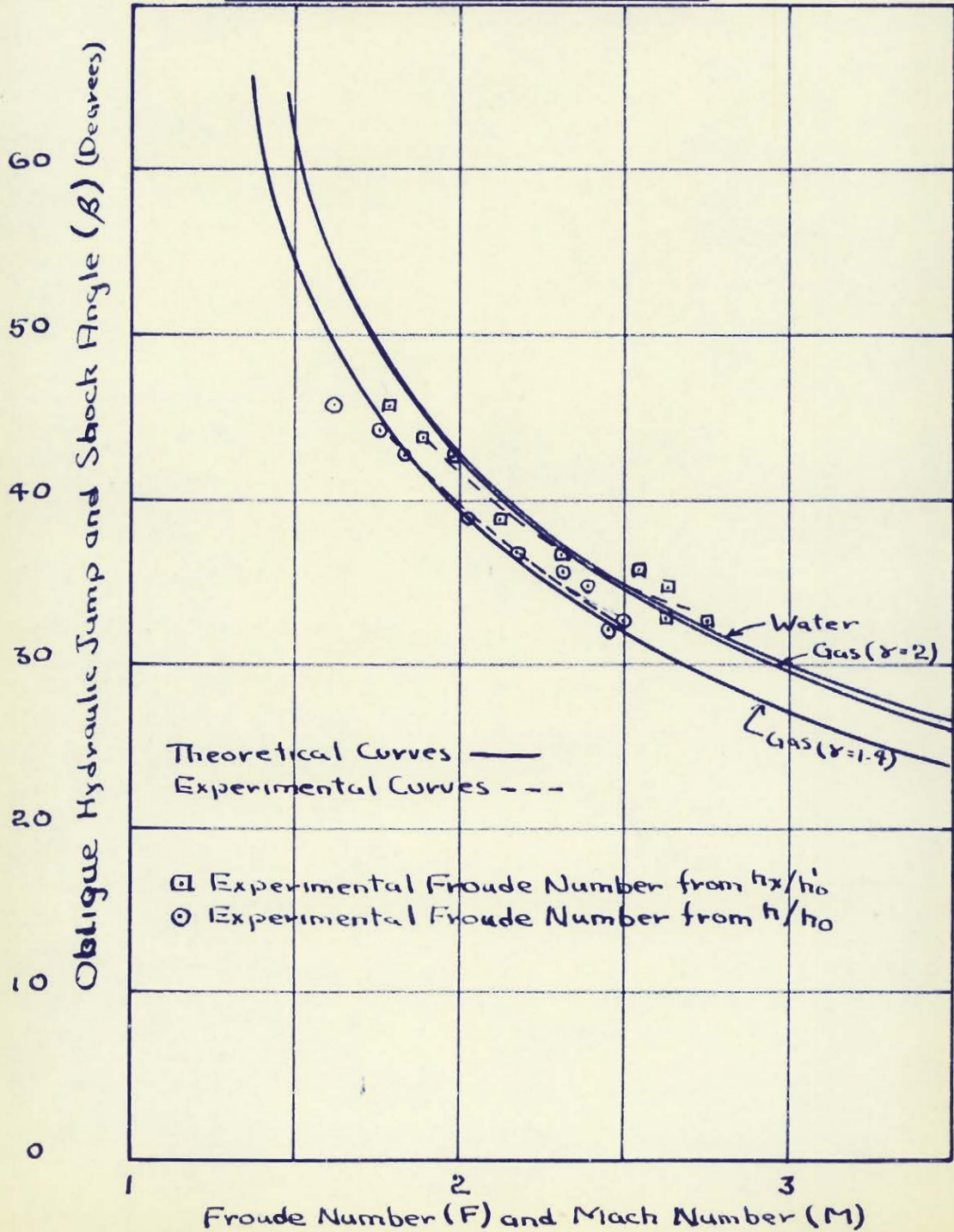


Figure 14

UPSTREAM FROUDE AND MACH NUMBER
VS
WIDTH AND AREA CONTRACTION RATIO
REQUIRED FOR SWALLOWING AN HYDRAULIC
JUMP AND SHOCK

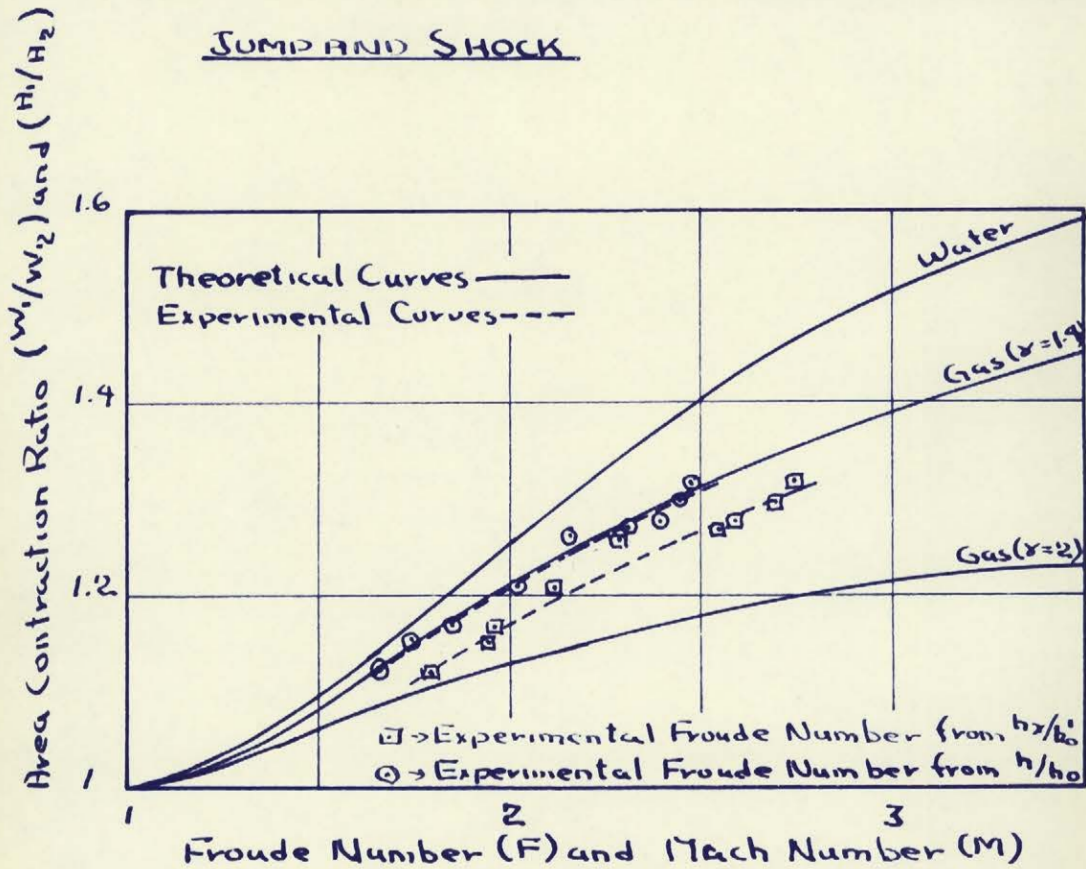


Figure 15

PERFORATED DIFFUSER

AREA CONTRACTION RATIO VS MASS FLOW RECOVERY FACTOR

- AT INLET FROUDE AND MACH NUMBERS

REQUIRED TO SWALLOW A SHOCK OR HYDRAULIC JUMP

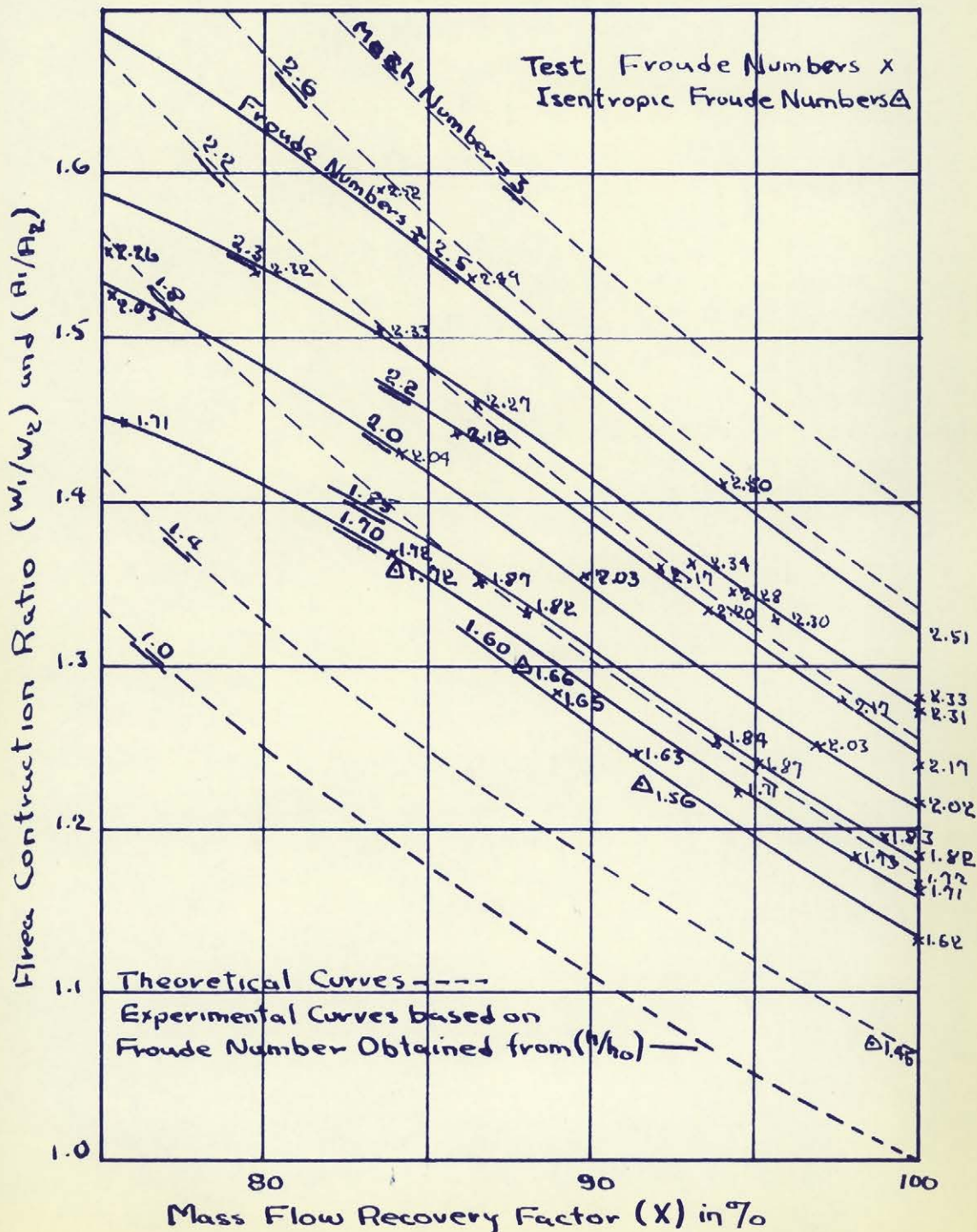


Figure 16

UPSTREAM FROUDE AND MACH NUMBER
VS
AREA CONTRACTION RATIO AND MASS FLOW RECOVERY
FACTOR → REQUIRED FOR SWALLOWING AN
HYDRAULIC JUMP OR SHOCK IN A PERFORATED DIFFUSER

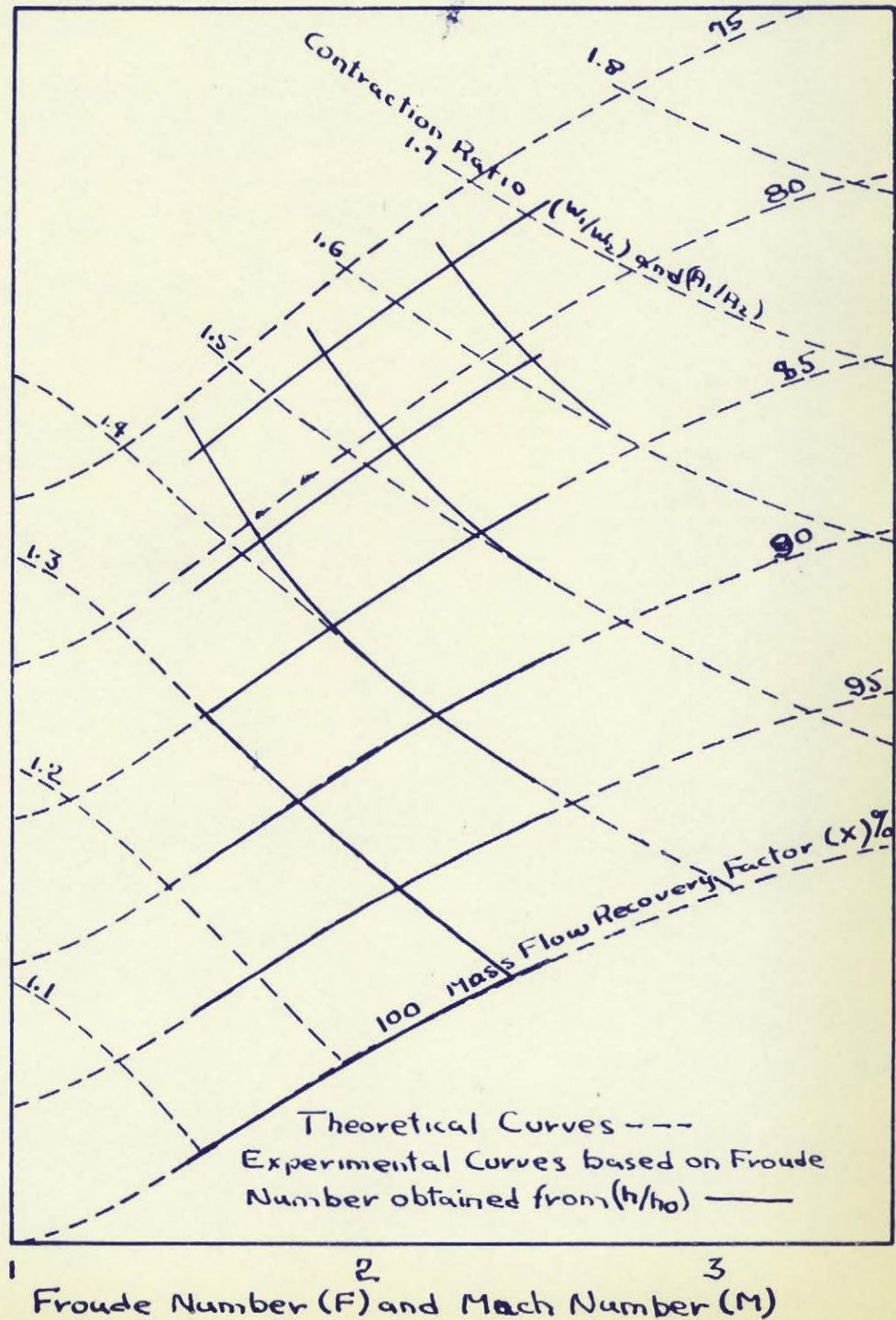
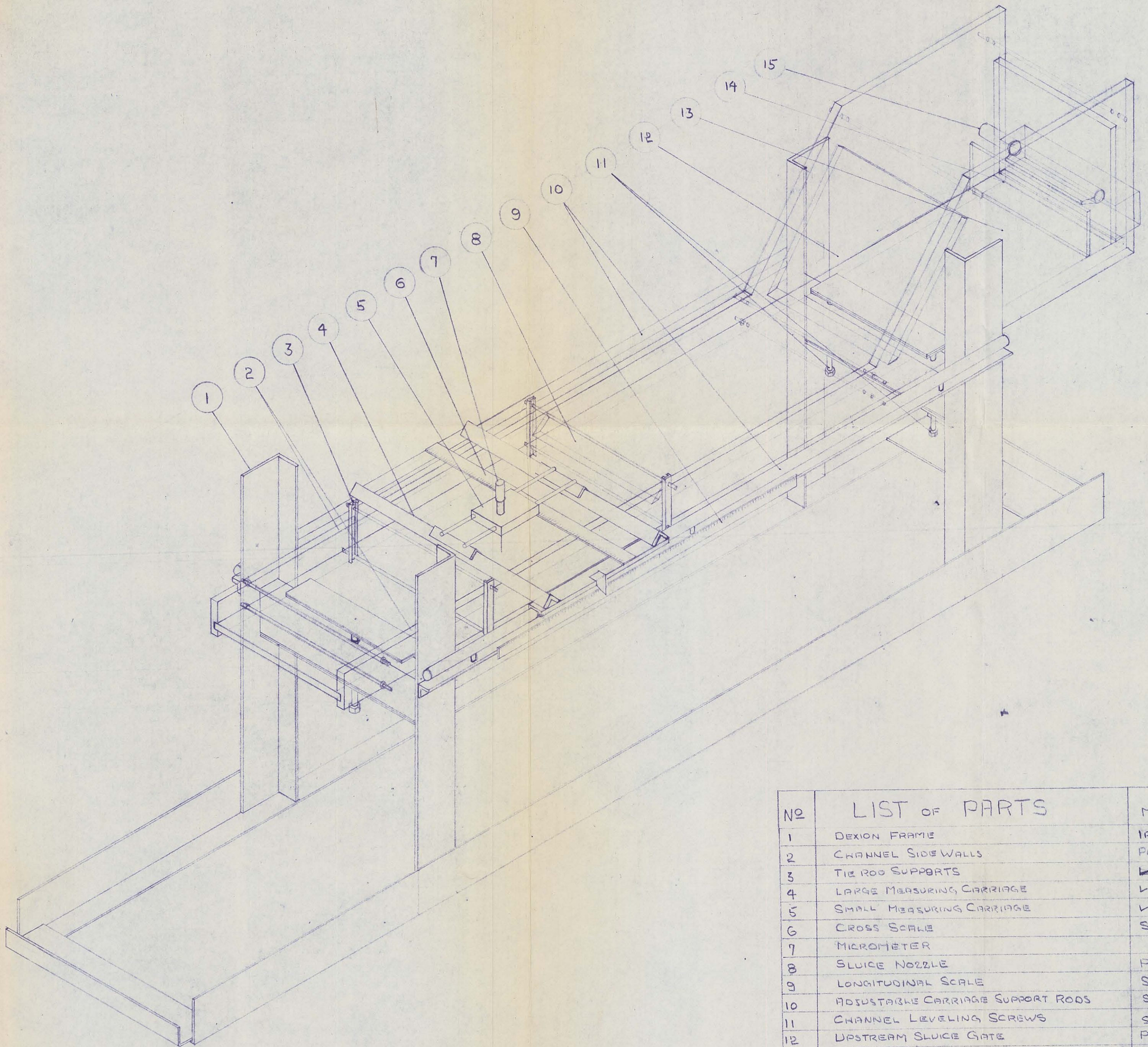


Figure 17

APPENDIX



NO	LIST OF PARTS	MATERIAL
1	DEXION FRAME	IRON
2	CHANNEL SIDE WALLS	PLASTIC
3	TIE ROD SUPPORTS	✓ IRON
4	LARGE MEASURING CARRIAGE	✓ IRON
5	SMALL MEASURING CARRIAGE	✓ IRON
6	CROSS SCALE	STEEL
7	MICROMETER	
8	SLUICE NOZZLE	PLASTIC
9	LONGITUDINAL SCALE	STEEL
10	ADJUSTABLE CARRIAGE SUPPORT RODS	STEEL
11	CHANNEL LEVELING SCREWS	STEEL
12	UPSTREAM SLUICE GATE	PLASTIC
13	CHANNEL BOTTOM	GLASS
14	ENTRANCE GATE	PLASTIC
15	WATER PIPE ENTRANCE	

ISOMETRIC
SCALE:
1" TO 5"

HYDRAULIC ANALOGUE

MCGILL UNIVERSITY
FEBRUARY 1960
C. J. Murphy